Modified 2D Finite-Difference Time-Domain Based Tunnel Path Loss Prediction for Wireless Sensor Network Applications

Yan Wu
Computer Laboratory, University of Cambridge, Cambridge, United Kingdom
Email: yw264@cam.ac.uk

Min Lin and Ian J. Wassell
Computer Laboratory, University of Cambridge, Cambridge, United Kingdom
Email: {ml406, ijw24}@cam.ac.uk

***Abstract*—To effectively deploy wireless sensor networks (WSNs) for monitoring and assessing the condition of tunnels, a Propagation Path Loss (PL) Model, which describes the power loss versus distance between the transmitter and the receiver for the tunnel environment is required. For most of the existing propagation measurements that have been conducted in tunnels, the antennas have been positioned along the central axis of a tunnel. However this is not representative of most infrastructure monitoring applications where the wireless sensor nodes will be mounted on the walls of the tunnel. In this paper, the results obtained from conducting close-to-wall measurements at 868MHz and 2.45GHz in curved arched-shaped tunnels are presented along with predictions made using a newly proposed Modified 2D Finite-Difference Time-Domain (FDTD) method. Since most currently available wireless sensor nodes have a communication range less than about 100m, we will focus on path loss measurement and modelling up to a maximum range of several hundred metres. During our measurements, the antennas are always maintained at a height of 2m, however the antenna distance to the tunnel wall is varied. By having the PL model as a guideline, we are able to determine the critical parameters for wireless communication in a tunnel, such as maximum communication distance, transmit power and receiver sensitivity.**

***Index Terms*—tunnel path loss, FDTD, large scale computing, field measurements**

I. Introduction

Having knowledge of the Path Loss (PL) versus distance characteristic for a particular civil infrastructure scenario avoids having to go back and repeat propagation tests if wireless nodes with different characteristics are deployed in the future. Therefore the determination of appropriate PL models enables effective Wireless Sensor Network (WSN) planning and deployment, for example in our case, to monitor and assess deformation in tunnels.

The increase of path loss with distance generally varies between 20 dB per decade for free space conditions and may exceed 50 dB per decade for a non-line of sight (NLOS) urban situation with very high building densities [1]. For modelling radio propagation in tunnels, a common approach is to treat them as a large scale waveguide. In [2], Zhang concluded that there are two propagation regions in a tunnel. The initial region exhibits path losses similar to that seen in free space followed by a region where the path loss gets worse more gradually since they act like oversized wave guides. In addition, the Modal Theory of electromagnetic (EM) propagation in rectangular or circular tunnels applied in [3] provides a reasonably accurate prediction of the periodic behaviour of the PL observed for antenna separations over a range of several kilometers. However, near distance PL accuracy is poor and close to wall antenna deployment is not amenable to prediction using this technique. To try and address these problems, a Ray Tracing technique has been employed in [4] to perform tunnel PL predictions, but unfortunately it does not provide the flexibility to cope with the variability of tunnel environments and also exhibits poor accuracy in some situations.

The Finite-Difference Time-Domain (FDTD) method proposed by Yee [5] has been serving the EM modelling community for more than 40 years. Although a huge amount of effort has been dedicated to improving this method, the conventional FDTD is still renowned for its stability and for being straight forward to implement. These issues are of fundamental importance for the large-scale EM simulation required in our situation. Even so, the truth is that it is almost impossible to perform a full 3D tunnel simulation using the conventional FDTD method since the computational cost is overwhelming to any regular personal computer (PC).

In this paper, we are going to present our field measurements for antennas mounted on the side wall of the tunnel and then propose the Modified 2D FDTD tunnel technique for generating PL predictions. The paper is organised as follows. The measurement equipment, procedures and the geometry of the initial tunnel investigated are introduced in Section II. Measurement results and analysis follows in Section III, including a further three tunnel field measurement scenarios. In Section IV, the Modified 2D FDTD model is presented

Manuscript received December 1, 2008; revised March 6, 2009; accepted March 23, 2009.

along with simulation results and comparisons with measured results. Finally, Section V draws our conclusions.

II. Field Measurement Setup

Our primary measurements are conducted at 868MHz and 2.45GHz within the Aldwych disused underground railway tunnel in London, which is 3.8m in diameter and 3.2m from the track bed to the crown. Fig. 1 gives a cross-sectional view of the tunnel. The side mounted transmitter was positioned close to the tunnel wall at the height of 2m (Ys), 0.02m (Xs) away from the wall and oriented vertically to the tunnel base. The use of a vertical antenna is to limit intrusion into the tunnel. Here we represent the side located transmitter position as T(Xs,Ys,Z0). The receiver position is represented as R(x,Ys,z), where x is the relative distance of antenna to wall separation; z is the distance along the tunnel from the reference distance Z0. For reference and comparison purposes, we also used a transmit antenna mounted at a height of 2m at the centre line of the tunnel.

At the receiver, the signal power is measured using a portable spectrum analyzer (SA) (Anritsu MS2721A) which is connected to a dipole antenna via a 10m low-loss coaxial cable. At the transmitter, AtlanTech ANS3-0800-001 (800~1200MHz) and AtlanTech ANS3-2000-001 (2000~3000MHz) battery powered signal generators are used. In addition, a Mini-Circuits power amplifier (PA) is used to increase the transmit power and a dipole antenna having an appropriate centre frequency is connected directly to the PA. The accuracy of this measurement setup has been validated in our plane earth measurements performed in [6]. Fig. 2 illustrates the 2D plan view of the tunnel while on the right hand side, two small circles represent the positions of the centre transmitter and the side transmitter antennas.

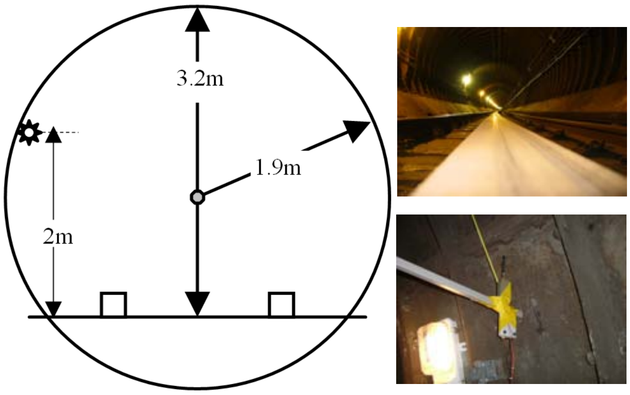

Figure 1. Aldwych Cross-Sectional View and Transmitter Position.

For each frequency, we carried out six sets of measurements in the Aldwych tunnel, which are described in Table 1. The measurement techniques used for each set of measurements is also indicated in the table. Two different measurement techniques are applied as will now be described:

a. A Low Resolution (LR) Technique, where measurements are conducted at intervals of 2m, 5m and 10m depending upon the transmitter to receiver separation and the operating frequency. At each measurement position, the transmitter is moved randomly within a 1 square meter area while 100 samples are recorded. By using this technique, the fading due to the strong multipath characteristics can be averaged out allowing the mean path loss to be estimated.
b. A High Resolution (HR) Technique, in which, the receiver is moved slowly and continuously along the

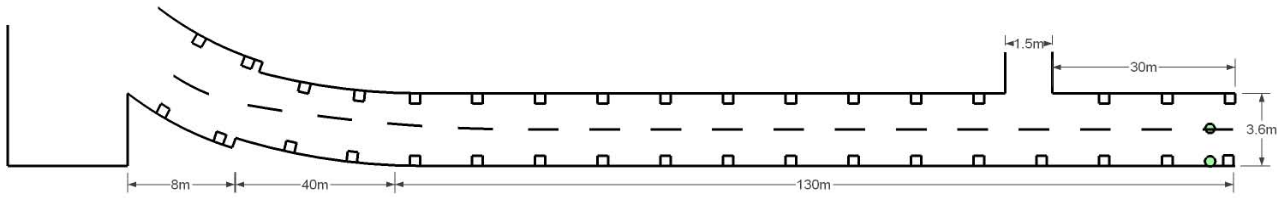

Figure 2. Aldwych 2D Geometry Plan and Transmitter Position.

Table 1: Six Sets of Measurements

	Set	Tx	Rx	Measurement
i	Centre to Centre (C-C): both transmitter and receiver are deployed at equal distance (noted as *Xc*) to both side walls	(X_c,Y_s,Z_0)	(X_c,Y_s,z)	LR & HR
ii	Side to Centre (S-C)	(X_s,Y_s,Z_0)	(X_c,Y_s,z)	LR & HR
iii	Side to Same Side 2cm (S-SS 2cm): receiver is 2cm away from the wall with transmitter mounted (noted as Wall S)	(X_s,Y_s,Z_0)	(X_{iii},Y_s,z)	LR
iv	Side to Same Side 11cm (S-SS 11cm): receiver is 11cm away from Wall S	(X_s,Y_s,Z_0)	(X_{iv},Y_s,z)	HR
v	Side to Opposite Side 2cm (S-OS 2cm): receiver is 2cm away from the wall opposite to Wall S	(X_s,Y_s,Z_0)	(X_v,Y_s,z)	LR
vi	Side to Opposite Side 11cm (S-OS 11cm): receiver is 11cm away from the wall opposite to Wall S	(X_s,Y_s,Z_0)	(X_{vi},Y_s,z)	HR

tunnel while the received signal strength is recorded at a rate of one sample per wavelength. This method provides us with detailed PL information against distance. In contrast to the LR method the measurement results still exhibit signal fading as a function of distance. It is not possible to take measurements at 2cm from the tunnel sides with any accuracy owing to flanges that protrude by about 10cm and other obstructions on the tunnel wall. Consequently, to obtain accurate results at closer spacings e.g., 1~2cm, the LR technique is more suitable.

III. Field Measurements results and analysis

The PL is defined differently in various contexts. To avoid confusion, here we define our PL in dB as:

$$PL_{(dB)} = P_{Tx(dBm)} + G_{Tx(dB)} + G_{Rx(dB)} - P_{Rx(dBm)} + P_{cable\_loss(dB)}, \quad (1)$$

where P_{Tx} is the transmit power; P_{Rx} is the receive power; P_{cable_loss} is the coaxial cable loss, which adds -1.5 dB at 868MHz and -2.0 dB at 2.45GHz; G_{Tx} and G_{Rx} are the transmit and receive antenna gain respectively (both are 2 dBi). From the LR measurements presented in Fig. 3, in general it can be seen that the PL increases more rapidly in the near region than in the far region of the tunnel. During previous tunnel PL studies, emphasis is often placed on the effect of key factors, such as operating frequency, tunnel material, shape and course. From our findings it is clear that antenna position is important, particularly in the WSN context. In the following sections, we will illustrate the effects owing to each factor.

A. Antenna Position

It can be seen from Fig. 3 that the PL worsens with side mounted antennas, specifically in the order C-C, Side Cases (i.e., S-C, S-SS and S-OS). In other words, more transmit power is needed using side mounted antennas to achieve the same coverage as for the C-C case. As can been seen in Table 1, the S-SS and the S-OS scenarios have been investigated for receive antenna to wall spacings of 2cm and 11cm. From the measurement results shown in Fig. 4, it can be seen that in general the 11cm spacing performs better than does the 2cm spacing. In other words, the close-to-wall receive antenna gives a worse overall performance. Note that for clarity, we only plotted one fifteenth of the samples collected from these HR measurements. We also added offsets to the plots of +60dB, +30dB, 0dB and -30dB in Fig. 4(a), (b), (c) and (d) respectively in order to conserve space. The detailed investigations in terms of antenna radiation patterns due to close to wall antenna spacings have been presented in [7]. In practical deployments, wireless sensors are often attached to walls with an antenna to wall spacing of less than 10 cm. In which case, it is important to consider the significant PL performance degradation owing to the antenna position. In [8], the practical issues encountered during various WSN field installations are described in detail.

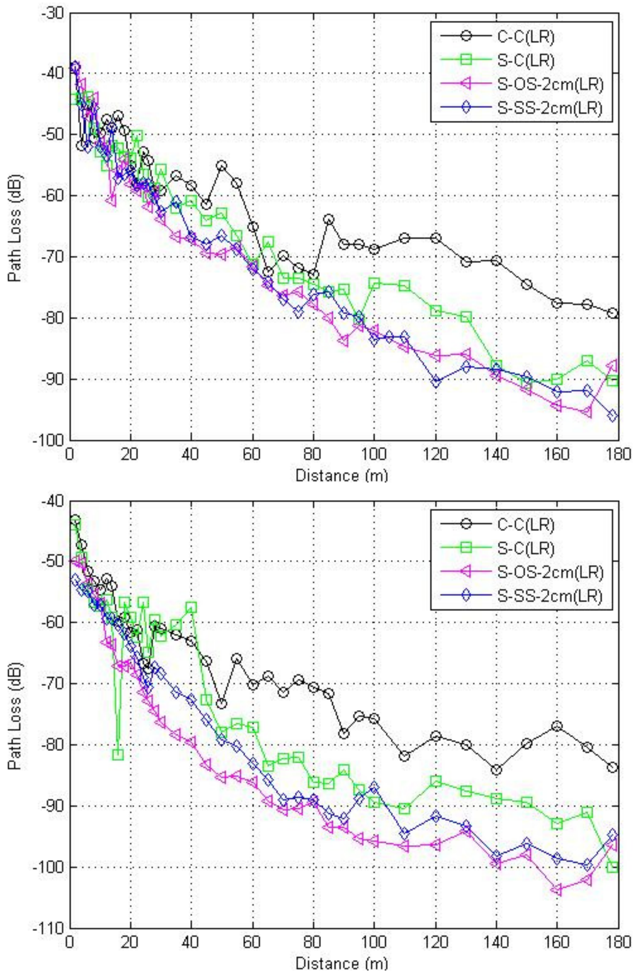

Figure 3. Aldwych PL Performance Comparison at Different Antenna Positions: Top Plot - 868MHz; Bottom Plot - 2.45GHz.

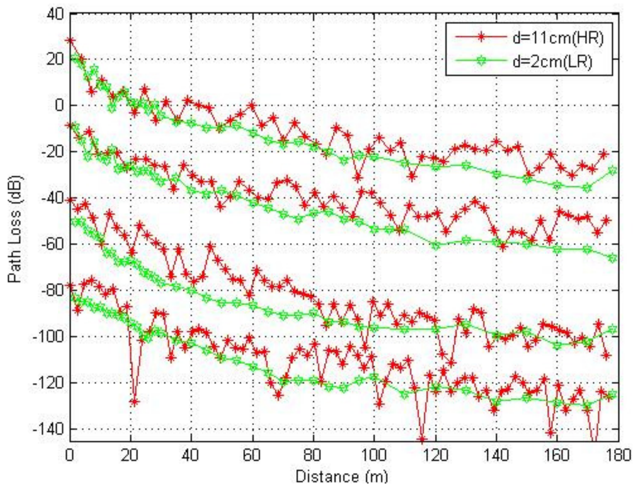

Figure 4. 2cm vs. 11cm Close-To-Wall Antenna Position Comparisons (from top down): a. (S-OS-2cm) vs. (S-OS-11cm) at 868MHz; b. (S-SS-2cm) vs. (S-SS-11cm) at 868MHz; c. (S-OS-2cm) vs. (S-OS-11cm) at 2.45GHz; d. (S-SS-2cm) vs. (S-SS-11cm) at 2.45GHz.

To confirm our conclusions, we have conducted further similar measurements in three different sections of the Bond Street underground railway tunnel in London shown in Fig. 5. Specifically we have: Bond T1 which is a straight 180m-long concrete tunnel from Ring no. 1984 to 2280; Bond T2 which is a curved 120m-long cast iron

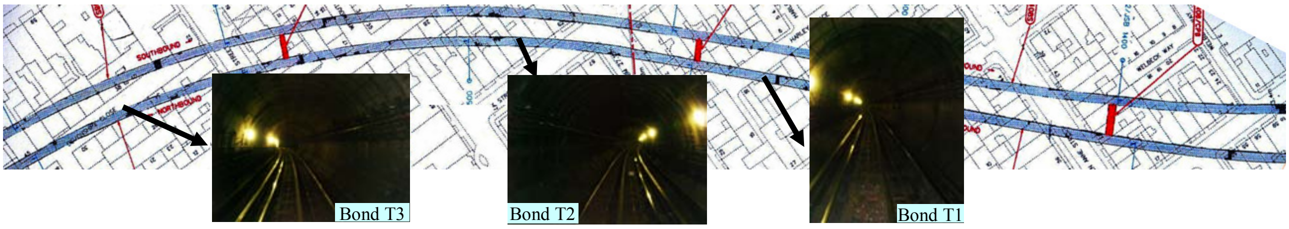

Figure 5. Bond Street Underground Railway.

tunnel from Ring no. 1782 to 1983 and Bond T3 which is a curved 108m-long concrete tunnel from Ring no. 1423 to 1603. Both Bond T2 and Bond T3 have the same radius of curvature and both lose Line of Sight (LOS) at a distance of approximately 45m. All of the three tunnel sections have an internal diameter of about 3.8m. Due to the constraint on working hours in operational London underground tunnels, we only carried out HR measurements in the Bond Street tunnel.

For clarity, we have only presented the C-C and S-OS HR results in Fig. 6, 7, 8 and 9 corresponding with Aldwych, Bond T1, Bond T2 and Bond T3 respectively. In terms of antenna positions, it can be seen that each sub-figure supports our previous proposition that at either frequency, regardless of the wall materials and the course, the C-C case always has a better PL than does the S-OS case. Note that all the S-OS cases in the various tunnels give similar results to their corresponding S-SS cases (not shown to conserve space).

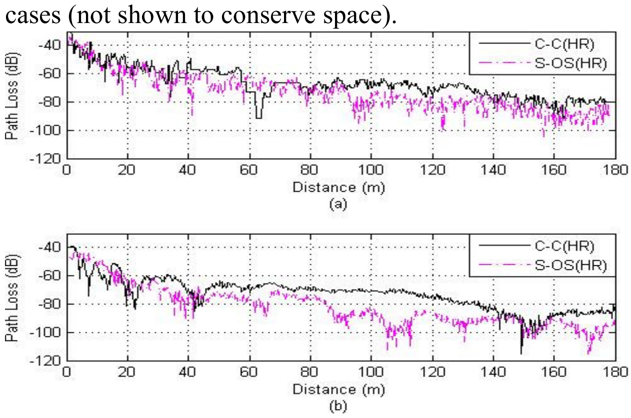

Figure 6. 868MHz PL HR Measurements in Two Straight Tunnels with Different Materials: (a). Aldwych Cast Iron C-C vs. S-OS, where its first 130m is straight; (b). Bond T1 Concrete C-C vs. S-OS.

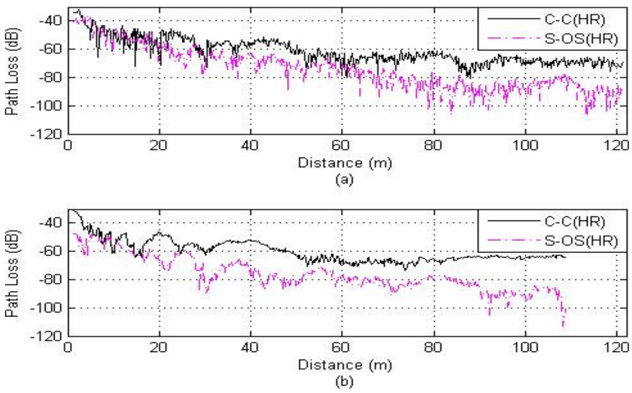

Figure 7. 868MHz PL HR Measurements in Two Curved Tunnels with Different Materials: (a). Bond T2 Cast Iron C-C vs. S-OS; (b). Bond T3 Concrete C-C vs. S-OS.

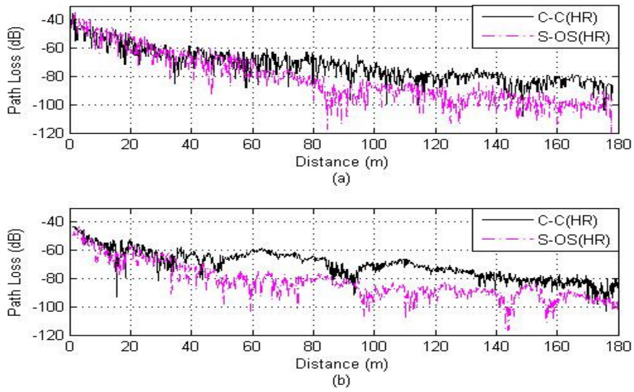

Figure 8. 2.45GHz PL HR Measurements in Two Straight Tunnels with Different Materials: (a). Aldwych Cast Iron C-C vs. S-OS, where its first 130m is straight; (b). Bond T1 Concrete C-C vs. S-OS.

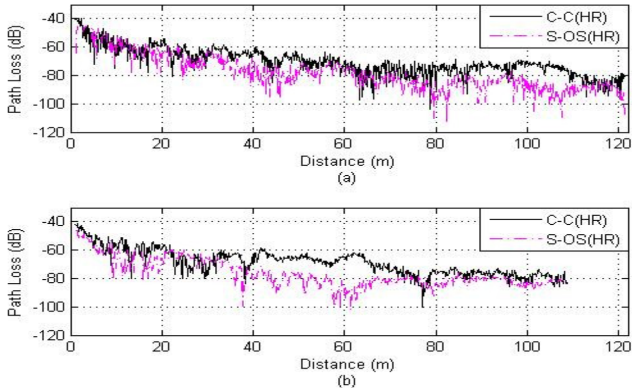

Figure 9. 2.45GHz PL HR Measurements in Two Curved Tunnels with Different Materials: (a). Bond T2 Cast Iron C-C vs. S-OS; (b). Bond T3 Concrete C-C vs. S-OS.

B. Tunnel Material and Course

In terms of the wall materials of a tunnel, we observed from our measurements that operating at a frequency of 868MHz, cast iron gives a noticeably better PL performance than does concrete, while at an operating frequency of 2.45GHz, the PL performances are very similar in both materials. Fig. 10 illustrates the surfaces of the cast iron and concrete sections. It can be seen that at either operating frequency, the cast iron tunnel measurements exhibit far more fast fading than do those in the concrete tunnel, owing to the surface roughness caused by the flanges between each cast iron segment. In addition, the cast iron material itself gives low loss reflections at close distances, which again gives rise to deeper fading.

In terms of the course of a tunnel, it is seen not to have a large impact on the PL performance at close ranges, although we note that straight tunnels yield slightly better results than do the curved ones, especially for non-LOS conditions.

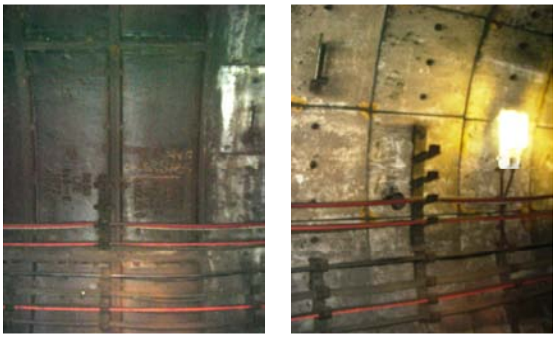

Figure 10. Cast Iron Lining (Left) and Concrete Lining (Right).

Within this paper, we only consider arched cross-section tunnels, however we would expect that the cross-sectional shape of a tunnel will affect the structural fading within the PL results but may still yield a similar mean PL performance. Some discussions concerning the effect of cross-section shape are presented in [4, 9].

C. *Operating Frequency*

In [10], it is shown that at higher operating frequencies, lower signal attenuation i.e., better PL performance can be achieved at long distances (i.e., several kilometers) in a tunnel. However, based on our results at the communication ranges of interest to us (i.e., several hundred metres at most), we will show that the previous conclusion does not apply. We discovered that we can describe the general trends for close range communication based on investigation of the C-C case and the Side Cases.

a. C-C Case

In Fig. 3, it can be observed that the C-C case operating at 868MHz gives a better PL performance than at 2.45GHz for antenna separations up to 180m. We also noticed that as the antenna separation approaches 180m that the PL at 868MHz tends to worsen at a faster rate than is evident at 2.45GHz. Consequently beyond this distance, it may be expected the PL at these two frequencies will reach the point of equality and then at even greater distances, 2.45GHz will have a better mean PL performance than does 868MHz. To be more specific, we would expect better PL performance for a lower operating frequency at close ranges (i.e., several hundred metres) and worse PL performance at longer distances (i.e., several kilometers).

So for the communication range likely to be experienced in a WSN deployment, operating at 868MHz will give a better PL performance than at 2.45GHz for the C-C case. This is probably owing to the fact that diffraction losses will be greater at 2.45GHz owing to the smaller wave length involved, i.e., 12cm compared with 35cm. This also means that we would expect less fast fading to be evident on the measurement results at 868MHz compared with those at 2.45GHz, and indeed this is what we observe. On the other hand, for general wireless communication over longer range, we would recommend higher operating frequencies, e.g., 2.45GHz for the reasons described previously.

In Fig. 11, we have presented a series of PL comparisons between 868MHz and 2.45GHz for the C-C case. We also added the offsets of 0dB, -40dB, -80dB and -120dB for Fig. 11(a), (b), (c) and (d) respectively in order to conserve space. It can be seen that in general 868MHz gives a better PL performance than does 2.45GHz in the C-C case.

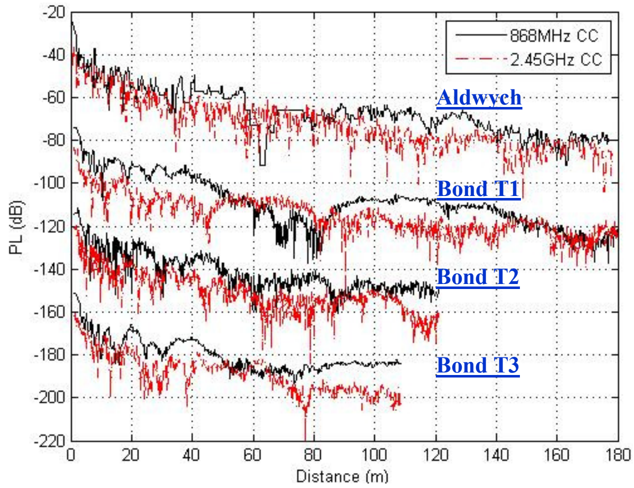

Figure 11. 868MHz vs. 2.45GHz C-C Cases Comparisons: (from top down): a. Aldwych Tunnel; b. Bond T1; c. Bond T2; d. Bond T3.

We also note a significant difference between the environment for the Aldwych measurements and that for the others, specifically the presence of a railway train approximately 120m behind the transmit antenna. To identify the effect of potential signal reflections from the train, we moved the train so that after the first and second moves it was 54.5m and 14.5m respectively behind our transmit antenna, yielding the results shown in Fig. 12.

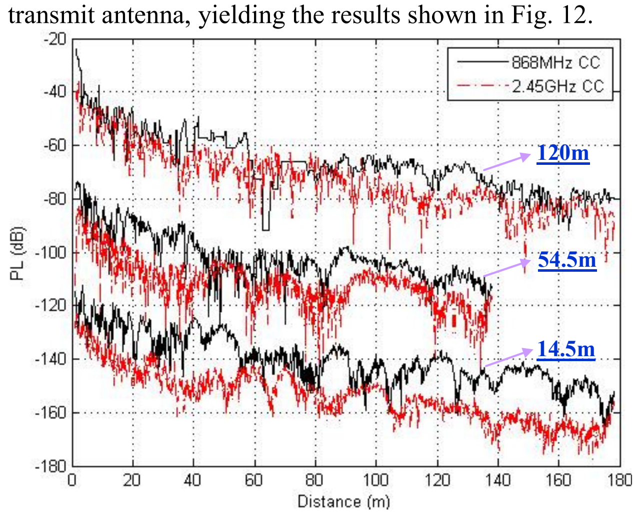

Figure 12. 868MHz vs. 2.45GHz C-C Cases when the Train is 120m, 54.5m (-40dB Offset) and 14.5m (-80dB Offset) away from the Transmit Antenna.

It can be seen in Fig. 12, that when the separation between the train and the transmitter decreases the PL gap between the 868MHz and 2.45GHz measurements increases. In fact, the PL performances at 868MHz and 2.45GHz both improve, but the improvement at 868MHz is more significant than that at 2.45GHz. This is probably because 2.45GHz has a wavelength of approximately

12cm compared with 35cm at 868MHz, which renders the front of the train a better reflector in the latter case. Consequently the reflections at 2.45GHz will be more scattered and more power will penetrate the gaps between the train and the tunnel wall, i.e., less power will be reflected back at 2.45GHz from the front of the train. We would anticipate similar effects due to the train for the corresponding side antenna cases.

b. Side Antenna Cases

Unlike the C-C cases where a significant difference exists between 868MHz and 2.45GHz PL performance for all tunnels at close antenna separations, in the side cases, the PL performance remains similar at both operating frequencies for all tunnels except Aldwych. Fig. 13 and Fig. 14 show comparisons for the SSS cases and for the SOS cases in Aldwych, Bond T1, T2 and T3 tunnels.

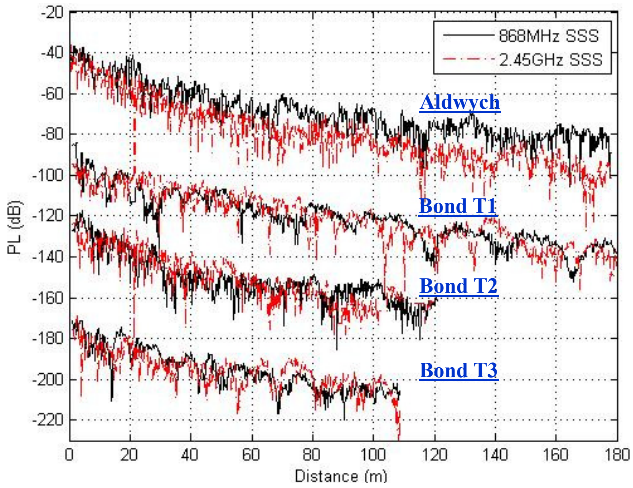

Figure 13. 868MHz vs. 2.45GHz SSS Cases Comparisons: (from top down): a. Aldwych (0dB Offset); b. Bond T1 (-40dB Offset); c. Bond T2 (-80dB Offset); d. Bond T3 (-120dB Offset).

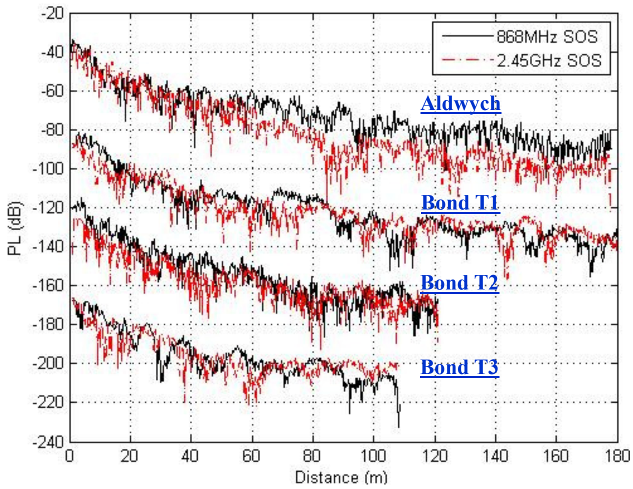

Figure 14. 868MHz vs. 2.45GHz SOS Cases Comparisons: (from top down): a. Aldwych (0dB Offset); b. Bond T1 (-40dB Offset); c. Bond T2 (-80dB Offset); d. Bond T3 (-120dB Offset).

Fig. 15 further investigates the Aldwych side antenna results in terms of the distance of the stationary train behind the transmit antenna. Once again, greater differences are evident between the PL performances at 868MHz and 2.45GHz. Consequently it may be reasonable to assume that when the tunnel passage is completely clear (as with all the tunnel measurements except for Aldwych), the difference between 868MHz and 2.45GHz for SSS and SOS case will be significantly reduced.

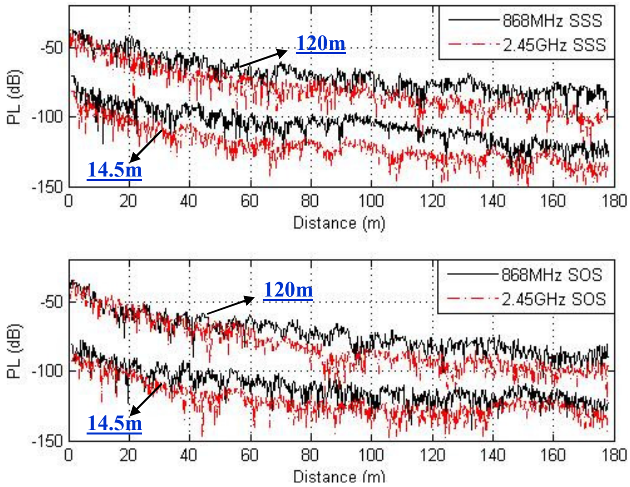

Figure 15. 868MHz vs. 2.45GHz SSS and SOS Cases when the Train is 120m and 14.5m (with -40dB Offset) away from the Transmit Antenna.

IV. MODIFIED 2D FDTD TUNNEL MODEL

By directly solving Maxwell's equations in the time domain, the FDTD method fully accounts for the effects of reflection, refraction and diffraction. The medium constitutive relation is incorporated into the exact solution of Maxwell's formulations. The advantages of the FDTD method are its accuracy and that it provides a complete solution for the signal coverage information throughout a defined problem space. Therefore it is well suited to the study of the Electromagnetic propagation in a complex environment.

Note that the FDTD requires memory to store the basic unit elements of the model and also demands iterations in time in order to update the fields along the propagation direction. In other words, excessively large computational power in terms of CPU execution time and memory usage are often needed for conventional FDTD approaches to large-scale problems. Indeed, for the axial distances of interest in our tunnel propagation scenarios, the problem space involved exceeds that of even the most sophisticated computing machines when implementing FDTD methods [11].

Consequently, the problem has become to see how we can convert a 3D tunnel model into a realistic 2D FDTD simulation, i.e., removing the computational burden while at the same time preserving the factors that shape the radio propagation characteristics. This has lead to our proposing the Modified 2D FDTD Method.

There are two conditions needed to convert a 3D FDTD into a 2D problem [12]: The property of the incident wave (signal source) and the property of the modeled structure. To make the transformation from 3D into 2D realistic, we will have to handle these two issues separately.

A. Signal Source Conversion and the Correction Factor

Previously in [13], we have considered free space and plane earth models, which both satisfy Taflove's structural descriptions for the 3D to 2D conversion. We note that in a 3D environment, the wave from a point source spreads out in a spherical manner. In contrast, we observe that in a plane, propagation occurs in a circular manner. The actual relationship between a 3D source and a 2D source in the FDTD technique has been revealed in terms of Correction Factor (CF), i.e.,

$$CF_{(dB)} = 10\log_{10}(R) + 10\log_{10}(f) - 23.2123, \quad (2)$$

where R is the distance between the transmitter and the receiver in m and f is the signal frequency in MHz. By subtracting the unique CF specified in (2) from the conventional 2D FDTD simulation results, we are able to achieve a close match between 2D FDTD simulation results and those expected in full 3D free space and plane earth models.

The CF can be conveniently determined because both the free space path loss model in (3) and plane earth path loss model in (4) have well-established analytical solutions as described in [14]:

$$PL_{(dB)} = 20\log_{10}(R/1000) + 20\log_{10}(f) + 32.4, \quad (3)$$

$$PL_{(dB)} = 10\log_{10}\left\{\left(\frac{\lambda}{4\pi R}\right)^2 \left|1 + \rho \exp\left(jk\frac{2h_t h_r}{R}\right)\right|^2\right\}, \quad (4)$$

where ρ is the reflection coefficient for the reflected ray; k is the free space wave number $2\pi/\lambda$. For example, ρ in the TE model is expressed as:

$$\rho_{TE} = \frac{(\sin\psi - \sqrt{(\varepsilon_r - jx) - \cos^2\psi})}{(\sin\psi + \sqrt{(\varepsilon_r - jx) - \cos^2\psi})}, \quad (5)$$

where x =18×109δ/f; ε_r is relative permittivity of the ground; δ is conductivity of the ground; ψ is the angle between the incident wave and the ground surface.

B. Structural Conversion and 2D FDTD Tunnel Model

Based on current understanding, it is known that antenna position, transmit frequency, tunnel diameter, building material and course are the main factors which affect radio propagation PL performance in a tunnel. Therefore our converted model has to at least take these factors into consideration as our conversion guidelines. Here we take the Aldwych tunnel as an example to illustrate the 2D FDTD model construction.

The 2D tunnel structure used in the FDTD simulations is that shown in the plan of the Aldwych tunnel given in Fig. 2. Fig. 16 illustrates the layout of the model in our simulation, where the TE(Ez,Hx,Hy) mode in the conventional 2D FDTD method is used to match our measurement setup, specifically the transmit and receive antennas are parallel to the tunnel wall and perpendicular to the tracks. In this model, all the parameters are preserved, i.e., tunnel diameter, wall material, flanges (if the wall is made of cast iron segments), tunnel course and the antenna positions relative to the wall. Similarly, we have also created FDTD models for Bond T1, Bond T2 and Bond T3 tunnels.

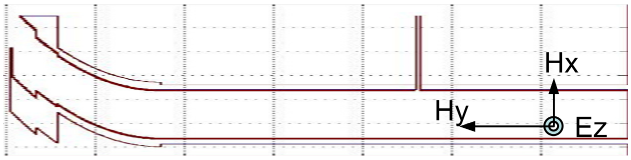

Figure 16. Modified 2D FDTD Aldwych Tunnel Structure.

To maintain the simulation accuracy, our unit cell size is defined to be equal to one twentieth of the corresponding frequency wavelength, i.e., 1.73cm at 868MHz and 0.61cm at 2.45GHz. In terms of the physical constants at each unit cell, cast iron lining is represented as (ε_r = 1.0, μ_r = 1.0, σ = 20×10^3), (ε_r = 7.0, μ_r = 1.0, σ = 0.015) for concrete lining and (ε_r = 1.0, μ_r = 1.0, σ = 0) for air. The 2D FDTD implementation is mainly based on [15]. To ensure that our simulation is close to steady state before our field sampling begins, we set the number of time steps to be 8 times larger than the time steps needed for the FDTD to cover the entire length of the tunnel.

C. Tunnel CF

So far we have shown how to transform a 3D into a 2D point source for free space and flat earth models, and have also proposed how a 3D tunnel structure can be represented in a 2D FDTD simulation. However, neither PL analytical formulations nor proven simulation models are available for us to determine the tunnel CF as we did previously for the free space and plane earth scenarios, particularly for close to wall antenna situations.

In order to find a suitable CF for this scenario, we have utilised the field measurements presented previously in this paper. Having results from four different tunnels with a total of 38 sets of field measurements, we have conducted investigations to determine the appropriate CF.

We will assume that the CF for our Modified 2D FDTD tunnel model for each measurement case has the same general form that applied previously, i.e.,

$$CF_{(dB)} = a\log_{10}(R) + b\log_{10}(f) + c, \quad (6)$$

where a, b, and c are the unknown variables, which we have seen for the free space and plane earth models are: a = 10, b = 10 and c = -23.2123.

Each variable of (a, b, c) is assumed to lie between 0 and 100. The Mean Square Error (MSE) between the measurement results and the corrected simulation results are calculated accordingly with various (a,b,c) combinations. We now have 38 3D matrices of the overall MSEs for the 38 cases. By searching for the (a,b,c) combinations which yield the 1500 lowest variances (out of the one million possible combinations) in each matrix, we reveal the ranges of interest for (a,b,c) and the corresponding range of variance values as shown in Table 2. We have listed only 24 sets from our analysis in order to conserve space. From Table 2, we realise that there are common values for (a,b,c) among all the cases, i.e., $18 \le a \le 20$; $4 \le b \le 29$; $3 \le c \le 95$, which indicate that we may be able to produce a unique CF for the general Modified 2D FDTD tunnel models.

TABLE 2: RANGE OF *(A,B,C)* YIELDING THE LOWEST CORRESPONDING VARIANCES IN EACH CASE

Aldwych	868MHz: (*a*,*b*,*c*,variance)
- CC	[18, 20]; [3, 35]; [-1, -95]; [7.72, 7.73]
- SSS	[14, 20]; [3, 38]; [-1, -100]; [8.81, 8.87]
- SOS	[18, 25]; [1, 37]; [-1, -100]; [8.35 ,8.47]
	2.45GHz: (*a*,*b*,*c*,variance)
- CC	[14, 20]; [2, 33]; [-1, -100]; [7.61, 7.70]
- SSS	[18, 31]; [1, 33]; [-1, -100]; [9.41, 9.77]
- SOS	[18, 37]; [1, 33]; [-1, -100]; [8.75, 9.77]
Bond T1	868MHz: (*a*,*b*,*c*,variance)
- CC	[18, 20]; [3, 36]; [-3, -100]; [7.86, 7.87]
- SSS	[9, 20]; [1, 39]; [-1, -100]; [7.83, 8.11]
- SOS	[18, 20]; [1, 34]; [-3, 100]; [8.50, 8.51]
	2.45GHz: (*a*,*b*,*c*,variance)
- CC	[11, 20]; [1, 32]; [-1, -100]; [7.34, 7.56]
- SSS	[18, 23]; [1, 29]; [-1, -100]; [8.46, 8.54]
- SOS	[18, 24]; [1, 30]; [-1, -100]; [7.60, 7.71]
Bond T2	868MHz: (*a*,*b*,*c*,variance)
- CC	[9, 20]; [1, 39]; [-1, -100]; [7.08, 7.35]
- SSS	[9, 20]; [3, 42]; [-1, -100]; [7.66, 7.94]
- SOS	[18, 26]; [1, 37]; [-1, -100]; [7.57, 7.72]
	2.45GHz: (*a*,*b*,*c*,variance)
- CC	[1, 20]; [1, 39]; [-1, -100]; [7.30, 8.28]
- SSS	[15, 20]; [2, 32]; [-1, -100]; [9.05, 9.10]
- SOS	[18, 20]; [4, 33]; [-3, -100]; [8.12, 8.13]
Bond T3	868MHz: (*a*,*b*,*c*,variance)
- CC	[7, 20]; [1, 39]; [-1, -100]; [6.57, 7.02]
- SSS	[7, 20]; [1, 40]; [-1, -100]; [6.23, 6.71]
- SOS	[9, 20]; [1, 39]; [-1, -100]; [6.92, 7.15]
	2.45GHz: (*a*,*b*,*c*,variance)
- CC	[18, 20]; [1, 29]; [-2, -97]; [7.09, 7.10]
- SSS	[3, 20]; [1, 37]; [-1, -100]; [7.59, 8.24]
- SOS	[5, 20]; [1, 37]; [-1, -100]; [6.97, 7.50]

By adding together all the 38 3D variance matrices of variance values, we now produce a single variance matrix for the entire tunnel model. The trend of the surface, which is defined by variable *c* and containing the minimum variance in the matrix is shown in Fig. 17.

The side view of Fig. 17 illustrates a smoothly curved plane with only a single turning point when it reaches the line of minima. Looking into the line of minima with respect to variables *a* and *b* independently as shown in Fig. 18, the problem of determining (*a*,*b*,*c*) is always deterministic, and there is only one set of (*a*,*b*,*c*) that yields the best fit CF for our 2D FDTD tunnel model.

To achieve better numerical accuracy for (*a*,*b*,*c*), we further refine the range containing the line of minima. Consequently the optimal set of (*a*,*b*,*c*) for the minimum overall variance is obtained and so the CF can be expressed as:

$$CF_{(dB)} = 18.4\log_{10}(R) + 4\log_{10}(f) - 8.0\,. \tag{7}$$

During our initial work when only the Aldwych measurement data was available, we took the same approach that we have just described in this section. The resulting CF formula for the 2D FDTD tunnel model was expressed as:

$$CF_{(dB)} = 20\log_{10}(R) + 8\log_{10}(f) - 19\,, \tag{8}$$

which also lies around the line of minima previously shown in Fig. 17 and Fig. 18.

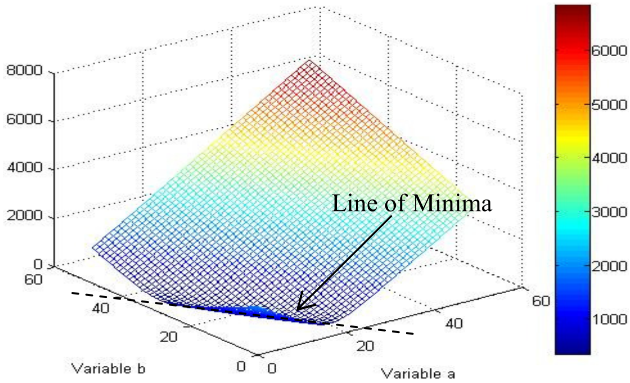

Figure 17. Overall Variance for Tunnel Model 3D View, for *c* = -8.0.

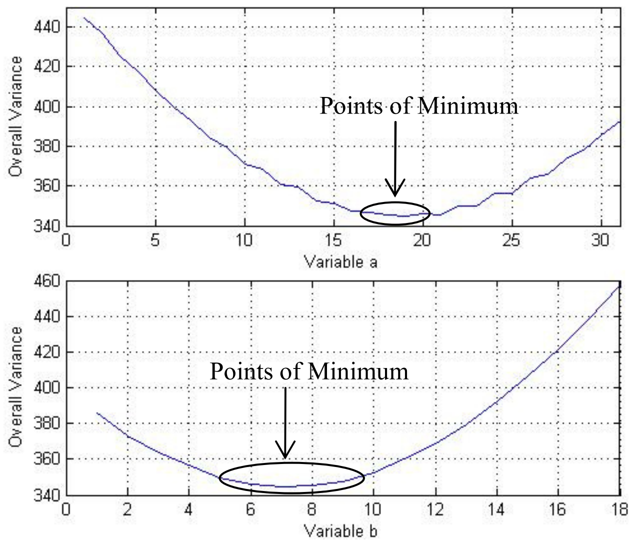

Figure 18. Observations from Variables *a* and *b*.

D. Evaluation

The Modified 2D FDTD tunnel PL predictions are obtained by subtracting the CF from the original 2D FDTD simulation data. A close correspondence between the measurement results and our simulation results can be seen in Fig. 19 for the Aldwych examples, which shows that the newly proposed CF for tunnels is appropriate for correcting conventional 2D FDTD results so that they represent measurements conducted in a full 3D environment.

The FDTD simulation has a very high resolution compared with the measurements, i.e., of the order of 10^4 samples in the simulation, $10^2 \sim 10^3$ in the HR measurements and much less in the LR measurements. The average root mean square (rms) error between the simulation and measurement results for all 38 scenarios conducted are shown in the 2nd column in Table 3. By applying a window filter, the simulation results are reduced to the same resolution as the measurements. This second comparison shows a much reduced rms error as shown in the 3rd column. In reality, we are interested in quantifying the prediction error for the mean path loss. Consequently to remove the fading effects, we applied window filters with an averaging window size up to 100 samples both to the simulation and to the measurement data. As a result, the rms error is further reduced as shown in the 4th column of Table 3.

TABLE 3: COMPARISONS OF RMS ERROR (DB) FOR THE MODIFIED 2D FDTD TUNNEL MODEL

CF of (a, b, c)	First Comparison	Second Comparison	Third Comparison
Initial Set (20, 8, -19)	9.7	5.6	3.9
Final Set (18.4, 4, -8)	9.0	5.2	3.6

There are several issues that we want to address in terms of the rms errors. Concerning the simulation, the total number of time steps for the FDTD iteration may not be large enough to cover the multipath effect at the far end of the tunnel, therefore we may expect larger errors to occur toward the far end. In terms of the way that we construct our FDTD model, we are effectively dealing with a 2D environment rather than 3D, which means the structural fading caused by the tunnel, will not be fully represented in the modified model and may affect the distribution of the fast fading data. Future work will investigate the fading statistics from the simulation data to see how it compares with that obtained from the measurements.

The simulation results reinforce our conclusions concerning the effect of each of the factors, i.e., antenna position, operating frequency, tunnel material and course, which were drawn in Sections III.A, III.B and III.C. As part of our future work, we plan to visit more tunnels having different dimensions in order to further validate our proposed Modified 2D FDTD tunnel model.

Note that our 2D FDTD simulations were performed on a 3.46GHz, 8GB RAM, Dell Precision PWS 380 computer. The current simulation time for 868MHz investigations is approximately 15 hours, rising to 90 hours for 2.45GHz, which can be further reduced by about 70% with the use of our Segmented FDTD method proposed in [16].

V. CONCLUSIONS

For WSN applications, we have shown that the PL worsens with side mounted antennas. The mean PL also becomes worse at short antenna separations when the operating frequency is increased, which is particularly relevant when implementing WSNs that usually have short expected communication ranges. Although material and course are also important elements to consider in tunnel radio propagation for WSNs, i.e., the short range situation, they have a less significant impact than do antenna position and operating frequency.

Based on our extensive measurement results, we have been able to develop our Modified 2D FDTD tunnel model, which can be employed to predict the PL performance at short ranges (i.e., several hundred metres) and for antennas that are positioned close to the tunnel

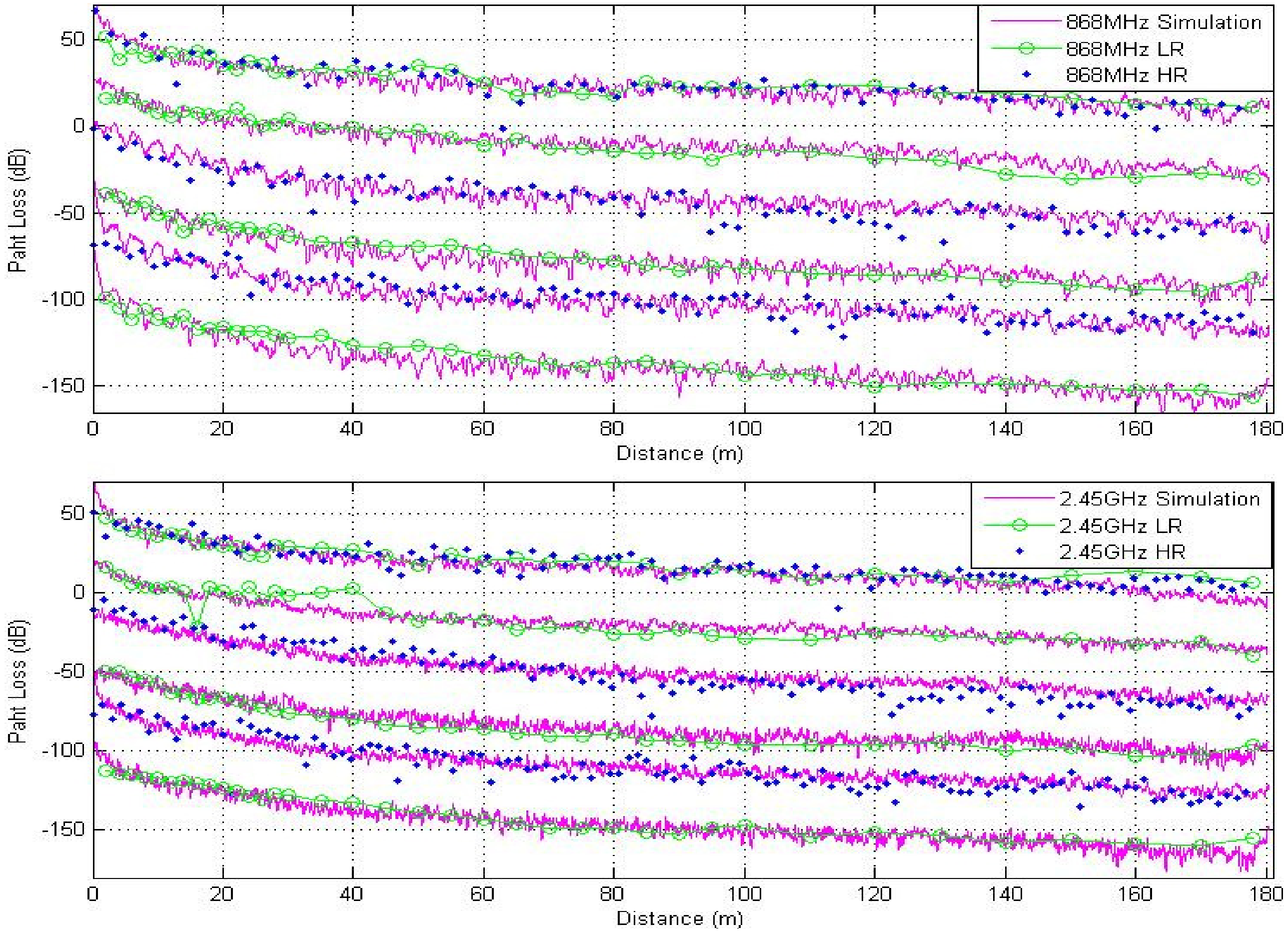

Figure 19: Aldwych 868MHz and 2.45GHz Evaluations (from top down in each subfigure): a. C-C (+90dB Offset); b. S-C (+60dB Offset); c S-OS 11cm (+30dB Offset); d. S-OS 2cm (0dB Offset); e. S-SS 11cm (-30dB Offset); f. S-SS 2cm (-60dB Offset).

wall. The proposed modelling technique has been shown to have a reasonable accuracy, particularly for estimating the overall mean PL.

ACKNOWLEDGMENT

The authors would like to acknowledge the financial support of the Engineering and Physical Sciences Research Council (EPSRC) titled Smart Infrastructure: Wireless Sensor Network System for Condition Assessment and monitoring of Infrastructure under Grant EP/D076870/1. The work described in this paper is an extension of that originally presented in [17].

REFERENCES

[1] D.J. Cichon, and T. Kurner, *COST Telecommunications – COST Action 231 Digital Mobile Radio Towards Future Generation Systems Final Report, Chapter 4, Propagation Prediction Models, COST 231 TD (95),* pp. 190-195, Sep. 2005.

[2] Y.P. Zhang, “Novel Model for Propagation Loss Prediction in Tunnels”, *IEEE, Trans. Veh. Technol.*, vol. 52, No. 5, pp. 1308-1314, Sep. 2003.

[3] J. M. Molina-García-Pardo, A. Nasr, M. Liénard and P. Degauque, “On the Possibility of Interpreting Field Variations and Polarization in Arched Tunnels Using a Model for Propagation in Rectangular or Circular Tunnels”, *IEEE Trans. Antennas Propag.*, vol. 56, No. 4, pp. 1206-1211, Apr. 2008.

[4] Dirk Didascalou, Jürgen Maurer and Werner Wiesbeck, “Subway Tunnel Guided Electromagnetic Wave Propagation at Mobile Communications Frequencies”, *IEEE Trans. Antennas Propag.*, vol. 49, No. 11, pp. 1590-1596, Nov. 2001.

[5] K.S. Yee, “Numerical Solution of Initial Boundary Value Problems involving Maxwell’s Equations in Isotropic Media”, *IEEE Trans. Antennas Propag.*, vol. 14, No. 3, pp. 302-307, May 1966.

[6] M. Lin, Y. Wu, I.J. Wassell, “Wireless Sensor Network: Water Distribution Monitoring System”, the *IEEE Radio & Wireless Symposium*, Jan. 2008.

[7] Y. Wu, M. Lin, and I.J. Wassell, “Investigation of Close-to-Wall Wireless Sensor Deployment using 2D Finite-Difference Time-Domain Modelling”, the *International Conference on Wireless Communication in Underground and Confined Areas*, Aug. 2008.

[8] Neil A. Hoult, Yan Wu, Ian Wassell, etc., “Challenges in Wireless Sensor Network Installation: Radio Wave Propagation”, *the International Conference on Structural Health Monitoring of Intelligent Infrastructure* (To Appear), Jul. 2009.

[9] T.-S. Wang, C.-F. Yang, “Simulations and Measurements of Wave Propagations in Curved Road, Tunnels for Signals from GSM Base Stations”, *IEEE Trans. Antennas Propag.*, vol. 54, No. 9, pp 2577~2584, 2006.

[10] Douglas O. Reudink, “Properties of Mobile Radio Propagation Above 400MHz”, *IEEE Trans. Veh. Technol.*, vol. VT-23, No. 4, pp. 143-159, Nov. 1974.

[11] Donald G. Dudley, “Martine Lienarcf, Samir F. Mahmoucf and Pierre Degauque, Wireless Propagation in Tunnels”, *IEEE Antennas Propag. Magazine*, vol. 49, No.2, pp. 11-25, Apr. 2007.

[12] Allen Taflove and Susan C. Hagness, Third Edition, *Computational Electrodynamics the Finite-Difference Time-Domain Method*, 2005.

[13] Y. Wu, M. Lin, I. J. Wassell, “Path Loss Estimation in 3D Environments using a Modified 2D Finite-Difference Time-Domain Technique”, *the IET 7th International Conference on Computation in Electromagnetics, CEM 2008*, pp. 98-99, Apr. 2008.

[14] Simon R. Saunders, *Antennas and Propagation for Wireless Communication Systems*, 2004.

[15] Dennis M. Sullivan, *Electromagnetic Simulation using the FDTD Method*, IEEE Press, Jul. 2000.

[16] Yan Wu, Ian Wassell, “Introduction to the Segmented Finite-Difference Time-Domain Method”, *the Biennial IEEE Conference on Electromagnetic Field Computation*, May 2008.

[17] Y. Wu, M. Lin, and I.J. Wassell, “Modified 2D Finite-Difference Time-Domain Technique for Tunnel Path Loss Prediction”, *the 2nd International Conference on Wireless Communication in Underground and Confined Areas*, Aug. 2008, Val-d’or, Canada.

Yan Wu was awarded the BEng degree in Computer Systems Engineering from the University of Warwick in June 2005. From September 2003 to August 2004, he held an industrial placement within the Storage System Division in IBM Hursley.

He has been a PhD candidate at the Digital Technology Group, Computer Laboratory, University of Cambridge since October 1, 2006. His research project is on "Smart Infrastructure: Wireless sensor network system for condition assessment and monitoring of infrastructure" sponsored by the Engineering and Physical Sciences Research Council (EPSRC). His main research focus is on EM based Propagation Modelling.

Min Lin obtained his BEng in Electrical and Electronic Engineering at University of Edinburgh in 2004. He has been a PhD candidate in Digital Technology Group, Computer Laboratory, University of Cambridge since October 2004.

From October 2004 to March 2006, he is working on MIMO channel modelling for Fixed Wireless Broadband Access, collaborating with Cambridge Broadband Laboratory. He is now working on channel modelling for wireless sensor network project, “Personalised Information from Prioritised Environmental Sensing (PIPES)”, funded by Department of Trading Industry (DTI) and BT.

Ian J. Wassell joined the University of Cambridge Computer Laboratory as a Senior Lecturer in January 2006. Prior to this appointment, he was with the University of Cambridge, Department of Engineering for approximately six and a half years.

He received the PhD degree from the University of Southampton in 1990 and the BSc., BEng. (Honours) Degrees (First Class) from the University of Loughborough in 1983. He has in excess of 15 years experience in the simulation and design of radio communication systems gained via a number of positions in industry and higher education. He has published more than 130 papers concerning wireless communication systems since joining the University of Cambridge in May 1999.

His research interests include broadband Fixed Wireless Access (FWA) networks, wireless sensor networks, radio propagation, coding and communication signal processing. He is a Member of the Institution of Engineering and Technology (IET).